Materials Research Bulletin 189 (2025) 113451

Contents lists available at ScienceDirect

Materials Research Bulletin

journal homepage: www.elsevier.com/locate/matresbu

Research Papers

Spectroscopy of Yb^{3+} ions in multisite $MgMoO_4$ crystal

Ghassen Zin Elabedine [a], Yana S. Didenko [b,c], Pavel Loiko [d], Kirill A. Subbotin [b,c], Anatolii I. Titov [b], Liudmila D. Iskhakova [b], Denis A. Lis [b], Sergei K. Pavlov [b,c], Yulia I. Zimina [b,c], Kristina V. Kuleshova [b,c], Rosa Maria Solé [a], Magdalena Aguiló [a], Francesc Díaz [a], Patrice Camy [d], Xavier Mateos [a,1,*]

[a] Física i Cristal·lografia de Materials (FiCMA), Universitat Rovira i Virgili (URV), Marcel·lí Domingo 1, 43007, Tarragona, Spain
[b] Prokhorov General Physics Institute of Russian Academy of Sciences, 38 Vavilova St., 119991, Moscow, Russia
[c] Mendeleev University of Chemical Technology of Russia, 9 Miusskaya Sq., 125049, Moscow, Russia
[d] Centre de Recherche sur les Ions, les Matériaux et la Photonique (CIMAP), UMR 6252 CEA-CNRS-ENSICAEN, Université de Caen Normandie, 6 Boulevard Maréchal Juin, 14050, Caen, France

ARTICLE INFO

Keywords:
Molybdate crystals
Czochralski method
Crystal structure
Ytterbium ions
Optical spectroscopy
Disordered crystals

ABSTRACT

Yb^{3+}-doped magnesium monomolybdate crystal (Yb:$MgMoO_4$) is grown by the Czochralski method. The crystal structure, thermal expansion, vibronic properties, polarized room- and low-temperature spectroscopy of this new compound were studied. According to the Rietveld refinement, Yb:$MgMoO_4$ belongs to the monoclinic class (sp. gr. *C*2/*m*, lattice constants: $a = 10.276(9)$Å, $b = 9.289(6)$Å, $c = 7.027(6)$Å and $\beta = 106.903(8)°$). The highest-energy Raman mode of Yb:$MgMoO_4$ is found at 969 cm^{-1} and assigned to symmetric stretching vibrations of $[MoO_4]^{2-}$ tetrahedra. Yb^{3+} ions in $MgMoO_4$ exhibit intense and broad absorption at 978 nm, relatively broad and smooth emission bands above 1 μm (stimulated-emission cross-section: $\sigma_{SE} = 0.76 \times 10^{-20}$ cm^2 at 1031 nm for light polarization $\boldsymbol{E} \parallel \boldsymbol{c}$) and a long luminescence lifetime (0.63 ms). The low-temperature (12 K) spectroscopic studies evidenced a multi-site behavior for Yb^{3+} ions in $MgMoO_4$ revealing at least 8 non-equivalent optical centers which are assigned to different charge compensation mechanisms. This induces a strong inhomogeneous spectral line broadening. For envisioned laser applications, the problem of low Yb^{3+} segregation coefficient (K_{Yb} ~0.029) needs to be solved.

1. Introduction

The development of ultrashort-pulse lasers around 1 μm based on Ytterbium (Yb^{3+}) ions requires the identification of promising gain media featuring both broadband emission properties and good thermal behavior. The spectral line broadening could be reached in crystals with a structure and / or compositional disorder however often at the expense of deteriorated thermal conductivity. It is also desired that laser gain materials provide linearly polarized emission to avoid the detrimental depolarization losses. The latter property could be attained for low symmetry matrices, *e.g.*, monoclinic crystals. Indeed, Yb^{3+}-doped ordered monoclinic (sp. gr. *C*2/*c*) double tungstate crystals $KRE(WO_4)_2$ (where RE stands for Y, Lu or Gd), are widely recognized for femtosecond mode-locked lasers and amplifiers at 1 μm [1,2]. Despite the appealing spectroscopic properties of these compounds, their main drawback stems from the relatively low thermal conductivity (~3 $Wm^{-1}K^{-1}$) [3] and impossibility to grow single crystals directly from melt [2].

Recently, ordered monoclinic (sp. gr. *P*2/*c*) magnesium and zinc monotungstate crystals, $MgWO_4$ [4–7] and $ZnWO_4$ [8–10], have been identified as interesting laser host matrices for doping with rare-earth ions (RE^{3+}), in particular, for broadly tunable and femtosecond mode-locked solid-state lasers [11,12]. These compounds combine i) rather good thermal conductivity [13]; ii) high birefringence [8]; iii) intense absorption and emission bands of RE^{3+} ions for polarized light [4,8]; iv) strong crystal fields resulting in large Stark splitting of RE^{3+} manifolds [14]; and v) efficient electron-phonon interaction [14] and Raman activity [15,16]. In particular, the room-temperature thermal conductivity of $MgWO_4$ amounts to 8.7 $Wm^{-1}K^{-1}$ [13]. Loiko et al. reported on a diode-pumped Yb:$MgWO_4$ laser delivering 18.2 W at ~1056

* Corresponding author.
E-mail address: xavier.mateos@urv.cat (X. Mateos).
[1] Serra Húnter Fellow, Spain.

https://doi.org/10.1016/j.materresbull.2025.113451
Received 14 December 2024; Received in revised form 10 March 2025; Accepted 24 March 2025
Available online 25 March 2025

nm with a slope efficiency of 89 % approaching the Stokes limit and a linearly polarized output [4]. Lin et al. developed an Yb:$MgWO_4$ oscillator mode-locked by a semiconductor saturable absorber mirror generating 125 fs pulses at 1065 nm at a repetition rate of 117 MHz and continuous wavelength tuning over 1019 – 1057 nm [11]. Recently, efficient laser operation of an Yb^{3+},Li^+ codoped $ZnWO_4$ crystal was also obtained: a continuous-wave Yb-laser generated 2.41 W at 1055–1058 nm with a slope efficiency of 76.4 % [17].

The origin of broadband emission properties of RE^{3+} dopant ions in $M^{2+}WO_4$ crystals (M = Mg, Zn) remained unclear: the authors claimed that it may originate from the complex doping mechanism involving univalent alkali-metal charge compensators, *i.e.*, Na^+ ions entering from the flux used for the growth of $MgWO_4$ [7] or Li^+ ions introduced intentionally in the case of $ZnWO_4$ [8,18]. In our recent study of Yb^{3+}-doped zinc monotungstate, we showed for the first time that even despite the ordered nature of this crystal (Zn^{2+} ions occupy a single 2*e* Wyckoff site with C_2 symmetry and VI-fold oxygen coordination), it presents a *multi-site* behavior as evidenced by the splitting of the Yb^{3+} absorption and emission zero-phonon lines observed at cryogenic temperatures [17]. This unexpected behavior was assigned to a variety of $Yb^{3+} \rightarrow Zn^{2+}$ substitutions and the associated local charge compensation, *e.g.*, involving vacancies or univalent alkali metal cations. Multi-site behavior has been recently evidenced for Er^{3+} ions in $ZnWO_4$ by laser site selective spectroscopy [19].

$MgWO_4$ melts incongruently, and, consequently, it is grown from the flux [7,20] resulting in relatively small crystals and tolerated optical quality. There exists its monomolybdate counterpart, $MgMoO_4$ [21–23] which melts congruently at 1322 °C [24] and can be grown by the standard Czochralski (Cz) method (from the melt) [25]. This compound crystallizes in the monoclinic class (sp. gr. *C*2/*m*, unit-cell parameters: a = 10.273(3)Å, b = 9.288(3)Å, c = 7.025(2)Å and β = 106.96° [26]) and exhibits a structure disorder due to existence of two non-equivalent sites for Mg^{2+} ions, labelled Mg1 (Wyckoff: *g*4*g*) and Mg2 (Wyckoff: 4*i*). Upon doping with RE^{3+} ions, it was suggested that they tend to replace the Mg^{2+} cations predominantly in one type of sites (Mg1) owing to the stronger distortion of the [$Mg1O_6$] octahedra and longer Mg1 – O interatomic distances [27]. However, this crystallographic behavior is expected to further promote the diversity of optical centers and induce additional inhomogeneous spectral line broadening, an effect being favorable for generation of ultrashort pulses.

$MgMoO_4$ was studied for scintillators as it exhibits broadband luminescence under irradiation by electron beam or α-particles [24,28]. Recently, this molybdate also attracted attention as a host matrix for doping with both transition-metal ions, notably Cr^{3+} [22] and rare-earth ions [23,29]. Recently, we reported on the growth, thermal and spectroscopic properties of Tm^{3+}:$MgMoO_4$ for emission at ~2 μm [23]. However, due to the complexity of crystal-field splitting of Tm^{3+} multiples, we were unable to conclude about the possible multi-site behavior of this compound.

In the present work, we report on the Czochralski growth, crystal structure refinement, Raman properties, and polarized room- and low-temperature spectroscopy of an Yb^{3+}-doped $MgMoO_4$ crystal with the goal of exploring promising structurally disordered compounds with broadband emission properties which are of interest for ultrafast lasers around 1 μm. Moreover, we present the first experimental evidence of multi-site behavior of RE^{3+}-doped magnesium monomolybdate.

2. Crystal growth and characterization techniques

2.1. Crystal growth

The starting materials for the growth of Yb-doped magnesium monomolybdate comprised MgO (purity: 4 N, Omskreactiv, Russia), MoO_3 (4 N, Lankhit Ltd., Russia), and Yb_2O_3 (YbO-D, 4 N, Industry Branch Standard 48–206–81, p/b M-5649 USSR). The Yb^{3+} concentration in the starting melt for Yb:$MgMoO_4$ growth was set to 7 at. % (considering the substitution of Mg^{2+} ions). First, the starting materials were thoroughly mixed and further calcined at a temperature of 700 °C during 5 h for solid-phase synthesis of the magnesium monomolybdate phase. Since the saturated vapor pressure of unbound MoO_3 at the melting point of $MgMoO_4$ exceeds 1 atm, a significant part of MoO_3 could evaporate from the melt if no calcining is applied prior to melting.

The single-crystal of Yb:$MgMoO_4$ was grown by the Cz method using a "Kristall-2″ growth station (USSR) in air atmosphere. A Pt/Rh crucible having a diameter of 30 mm and a height of 30 mm was used. The seed for the crystal growth was cut from undoped $MgMoO_4$ along the crystallographic axis [001]. During the growth, the pulling rate was 1 mm/h and the rotation speed was 6 revolutions per minute (r.p.m.). After completing the growth, the crystal was removed from the melt surface and slowly cooled down to room temperature (RT) using a rate of 8 °C/h with the goal of preventing the risk of cracking. The as-grown crystal was further annealed in air at 800 °C for 2 weeks to remove the stresses formed during the growth and improve its transparency.

2.2. Experimental

The actual Yb^{3+} concentration in the crystal was measured by the energy-dispersive X-ray spectroscopy (EDXS) (AZtecENERGY analytical systems; Oxford Instruments; JSM5910-LV, JEOL), at an accelerating voltage of 20 kV. The polished surfaces of the sample for the EDXS analysis was coated with a conducting carbon film. The analytical errors did not exceed 0.05, 0.12 and 0.10 wt % for Mg, Mo and Yb, respectively.

The phase purity of the investigated crystal was determined using X-ray diffraction (XRD) measurements in the θ - θ Bragg-Brentano configuration. The measurements were performed using a Bruker-AXS D8-Advance diffractometer and CuK_α radiation (λ = 0.15406 nm) at 40 kV and 30 mA, under room temperature conditions (293 K). The step scan rate was 3 s per step, with a step size of 0.05° over a 2θ range of 10 to 70 °. The XRD patterns of the sample were compared with the reference standard; the XRD data for undoped $MgMoO_4$ were represented by PDF card No. 72–2153.

High quality data are essential for crystal structure refinement, so we have performed additional XRD measurements using the variable-counting-time (VCT) technique to collect the data used for the Rietveld refinement. These measurements were made using the same Bruker-AXS D8-Advance diffractometer used in previous measurements, with a vertical θ - θ goniometer, incident- and diffracted-beam Soller slits of 2.5°, a fixed 0.5° receiving slit and an automatic air scattering knife on the sample surface. The angular 2θ range was between 12 and 90°. The data were collected with an angular step of 0.02° with a variable counting time from 1 to 14 s. The $Cu_{K\alpha}$ radiation was obtained from a copper X-ray tube operated at 40 kV and 40 mA. The diffracted X-rays were detected with a position sensitive detector (PSD) LynxEye-XE-T with an opening angle of 2.94°

The X-ray diffraction pattern of the sample measured using the VCT technique over a 2θ diffraction angle range of 12–-0° was analyzed and refined using the Rietveld method with the Topas V6 software. For the Rietveld refinement, the crystal structure of undoped $MgMoO_4$ (represented by PDF card No. 72-2153) was used as the starting model.

The linear thermal expansion tensor of Yb:$MgMoO_4$ was calculated taking into account the evolution of its unit-cell parameters with temperature. For this study, powder X-ray diffractograms from room temperature to 600 °C were recorded in the 2θ range from 5 to 80° with a temperature step of 50 °C, using the same diffractometer than in the previous measurements, but equipped with a modular temperature chamber (MCT-HIGHTEMP, Bruker). The heating rate was 10 °C/min and a delay time of 300 s was applied before doing the measurements. The diffraction data were recorded with an angular step size of 0.02° and a step time of 1 s. The unit-cell parameters were refined using the Pawley method with Topas V6 software.

For spectroscopic studies, the crystals were oriented with respect to

the crystallographic axes by means of single-crystal diffraction. The crystal orientation was performed using a Bruker-AXS D8-Discover diffractometer, with a parallel incident beam, a vertical θ - θ goniometer and a 3D motorized stage. A general area diffraction system (HI STAR detector) located at 15 cm from the sample was used. The measurements were carried out in the 2θ range from 8 to 92°

The polarized Raman spectra were acquired using a Renishaw inVia confocal Raman microscope employing an × 50 Leica objective, an edge filter, and an Ar^+ ion laser (λ_{exc} = 514 nm).

The absorption spectra for polarized light were recorded using a spectrophotometer (Lambda 1050, Perkin Elmer) and a Glan-Taylor polarizer. The luminescence of Yb^{3+} ions was excited by a tunable Ti: Sapphire laser and detected using a CaF_2 lens, a ZrF_4 fiber and an optical spectrum analyzer (OSA, Ando AQ-6315A). Low-temperature (LT, 12 K) spectroscopic studies were conducted using a APD DE-202 closed-cycle cryo-cooler equipped with an APD HC 2 Helium vacuum cryo-compressor and a Laceshore 330 temperature controller.

To study luminescence dynamics, we used a ns optical parametric oscillator (Horizon, Continuum), a 1/4 m monochomator (Oriel 77200), a fast InGaAs detector and an 8 GHz digital oscilloscope (DSA70804B, Tektronix).

3. Results and discussion

3.1. Results on the crystal growth

Fig. 1 presents a photograph of an as-grown Yb:$MgMoO_4$ single-crystal. The crystal boule has an amber-like coloration. The actual Yb^{3+} doping level in the crystal was determined to be 0.2 at. % (according to $Yb^{3+} \rightarrow Mg^{2+}$ substitution), and the ion density N_{Yb} was calculated to be 0.63×10^{19} at/cm^3. The segregation coefficient of Yb^{3+} ions, $K_{Yb} = C_{crystal}/C_{melt}$, where $C_{crystal}$ is the actual doping level in the crystal and C_{melt} is its nominal concentration in the melt, was estimated to be only ~0.029.

The entrance of trivalent rare-earth ions into the lattices of Mg^{2+}-based crystals is often very difficult. Indeed, for the Mg_2SiO_4 crystal, the segregation coefficient of Yb^{3+} ions was found to be as low as 0.001 [30]. Comparing the isostructural host crystals $MgWO_4$ and $ZnWO_4$, the Ho^{3+} distribution coefficient between the Ho:$MgWO_4$ crystal and the flux was found to be 0.086 [6], whereas the Yb^{3+} distribution coefficient between the related magnesium free Yb:$ZnWO_4$ crystal and the melt could reach the value of 0.5 [18]. In our previous studies focusing on magnesium monomolybdate doped with Tm^{3+} and Nd^{3+} ions, the corresponding segregation coefficients amounted to K_{Tm}= 0.02 [23], and $K_{Nd} < 0.01$ [25]. The reason for such behavior is not clear so far. It can be caused by substantial difference in the chemical nature between Mg^{2+} and trivalent lanthanides.

3.2. Crystal structure

The measured X-ray powder diffraction (XRD) pattern of the 0.2 at. % Yb:$MgMoO_4$ crystal together with the results of the Rietveld refinement are shown in Fig. 2. The results of the analysis indicate that all the observed diffraction peaks are consistent with the reference standard and no additional peaks indicative of impurities are observed, demonstrating the phase purity of the grown crystal. The refinement results show that Yb^{3+}:$MgMoO_4$ crystallizes in the monoclinic class. This compound belongs to the space group *C2/m* (point group 2/*m*) with a general multiplicity Z of 2. The refinement quality is evaluated using several reliability factors, including R_p = 8.8 %, R_{wp} = 11.71 %, and R_{exp} = 7.86 %, with a reduced chi-squared value of $\chi^2 = (R_{wp}/R_{exp})^2 = 2.22$. The lattice constants of the Yb^{3+}:$MgMoO_4$ crystal are determined to be a = 10.276(9)Å, b = 9.289(6)Å, c = 7.027(6)Å and β = 106.903(8)°, the unit cell volume V = 641.932(7) Å^3. The determined lattice constants are slightly exceeding those reported previously for undoped $MgMoO_4$ (a = 10.273 Å, b = 9.288 Å, c = 7.025 Å and β = 106.96°, V = 641.14 Å^3), and are close to those for the Tm^{3+}:$MgMoO_4$ crystal [23]. This difference between undoped and RE^{3+}-doped $MgMoO_4$ crystals occurs, obviously, due to the difference in the ionic radii between the host-forming cations, Mg^{2+} (0.72 Å) and the dopant ions, Yb^{3+} (0.868 Å), or Tm^{3+} (0.88 Å), respectively.

The calculated pattern demonstrates good agreement with the experimental data, as shown in Fig. 2. The calculated density of the crystal is ρ_{calc} = 3.816 g/cm^3. It is lower than that of Tm:$MgMoO_4$ (3.888 g/cm^3) [23]. The obtained fractional atomic coordinates (*x, y, z*), site occupancy factors (O.F.), and isotropic displacement parameters (B_{iso}) are listed in Table 1.

The crystal structure of Yb:$MgMoO_4$ is depicted in Fig. 3(a,b), which presents the projections of the structure along the ***b***- and ***c***-axes, based on the atomic coordinates determined through Rietveld refinement. The structure of Yb:$MgMoO_4$ can be described as a two-layered composition of MgO_6 polyhedra layers separated by MoO_4 polyhedra layers, as shown in Fig. 3(a). The distinct structural feature of Yb:$MgMoO_4$ is the criss-cross unit site, depicted in Fig. 4, in which the coordination environment of Mg(1) and Mg(2) ions is shown. The criss-cross unit site is formed by the interconnected MgO_6 polyhedra through common edges. The dopant Yb^{3+} ions preferentially replace the host-forming cations Mg^{2+} at one of the lattice sites, namely the Mg(1) site [31]. The structures of Yb^{3+} and Tm^{3+} doped $MgWO_4$ crystals are similar.

Fig. 1. A photograph showing an as-grown 0.2 at. % Yb^{3+}-doped $MgMoO_4$ crystal (actual doping). The growth direction is along the [001] axis.

3.3. Tensor of linear thermal expansion

The tensor of linear thermal expansion for the Yb:$MgMoO_4$ crystal in the crystallophysical system (with X_1 axis parallel to ***a***-axis, X_2 parallel to ***b***-axis and X_3 parallel to ***c****-axis) was characterized by monitoring the change of the unit-cell parameters with temperature. The tensor coefficients were calculated from the slope of the linear fits of the evolution of the normalized unit-cell parameters with temperature, see Fig. 5, according to the expression: $\alpha = (1/L_{30\,^\circ C})(\Delta L/\Delta T)$, where $L = a, b, c$ and $c \times \cos(\beta - 90^\circ)$.

Thus, the linear thermal expansion tensor in the crystallophysical system is:

$$(a_{ij}) = \begin{pmatrix} 7.365 & 0 & 0.226 \\ 0 & 14.00 & 0 \\ 0.226 & 0 & 3.869 \end{pmatrix} \times 10^{-6}\, K^{-1}. \quad (1)$$

By diagonalizing this tensor, the thermal expansion tensor in the eigen-frame is:

$$\left(a'_{ij}\right) = \begin{pmatrix} 7.380 & 0 & 0 \\ 0 & 14.00 & 0 \\ 0 & 0 & 3.854 \end{pmatrix} \times 10^{-6}\, K^{-1}, \quad (2)$$

with the principal axis $X_{1'}$ found at 3.69° from the ***a***-axis (clockwise), $X_{2'}$ being parallel to the ***b***-axis and $X_{3'}$ found at 13.21° from the ***c***-axis (anticlockwise). In this setting, the ***b***-axis is pointing towards the observer.

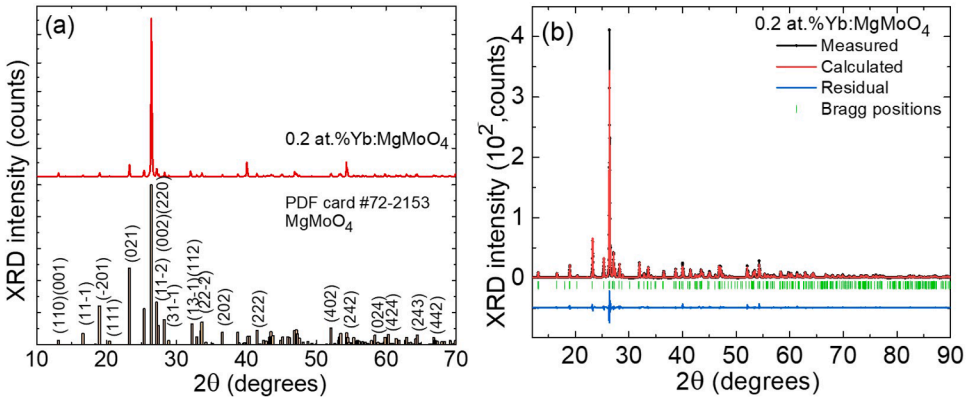

Fig. 2. X-ray powder diffraction (XRD) pattern for the 0.2 at. % Yb:$MgMoO_4$ crystal: (a) the measured XRD pattern, for comparison, the theoretical pattern for undoped magnesium monomolybdate (ICSD card No. 72–2153 [26]) is shown by vertical bars, *numbers* denote the Miller's indices (*hkl*) for the most intense reflections; (b) output of the Rietveld structure refinement: the measured (*black*), calculated (*red*) and residual (*blue*) profiles, *vertical dashes* mark the Bragg positions.

Table 1
Atomic coordinates, sites, occupancy factors (O.F.) and isotropic displacement parameters B_{iso}(Å^2) for 0.2 at. % Yb:$MgMoO_4$ crystal.

Atoms	*x/a*	*y/b*	*z/c*	O.F.	B_{iso}, Å^2	Wyckoff	Symmetry
Mg1	1/2	0.1781	0	0.998	0.989(7)	4*g*	2
Yb	1/2	0.1781	0	0.002	0.989(7)	4*g*	2
Mg2	0.7973	1/2	0.6396	1	0.290(5)	4*i*	*m*
Mo1	1/2	0.2517(3)	1/2	1	0.962(2)	4*h*	2
Mo2	0.7290(5)	1/2	0.0956	1	0.947(3)	4*i*	*m*
O1	0.5420(7)	0.1538(4)	0.3010(6)	1	0.284(3)	8*j*	1
O2	0.3613(2)	0.3560(6)	0.3917(8)	1	1.042	8*j*	1
O3	0.8563(8)	1/2	0.9609(4)	1	1.089	4*i*	*m*
O4	0.6336(8)	0.3449(4)	0.0252(9)	1	0.507(1)	8*j*	1
O5	0.2961(2)	0	0.3554(6)	1	1.943	4*i*	*m*

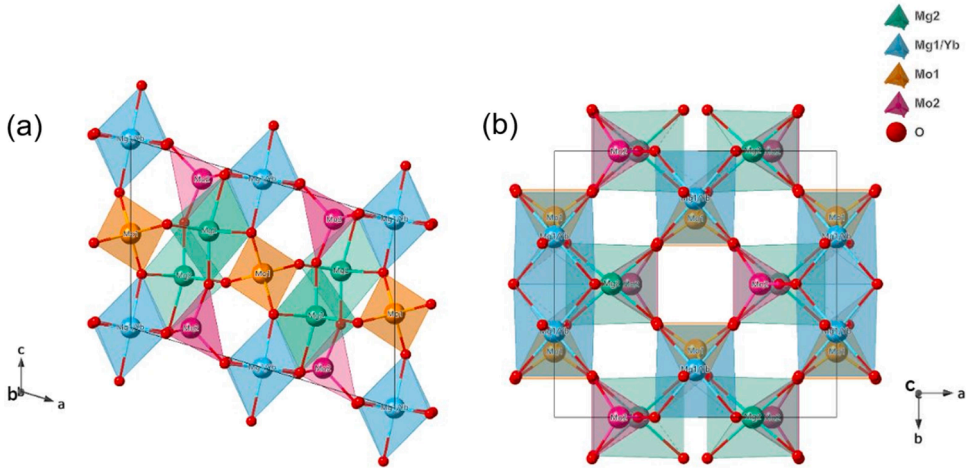

Fig. 3. (a,b) The structure of 0.2 at. % Yb:$MgMoO_4$: (a) projection in the ***a*-*c*** plane; (b) projection in the ***a*-*b*** plane; *black lines* – unit-cell.

3.4. Raman spectra

Yb:$MgMoO_4$ crystallizes in a monoclinic structure, space group *C*2/*m*, with 8 molecules per unit cell. The factor group theory analysis predicts that the optical modes are distributed among the irreducible representations of the factor group C_{2h} at the center of the Brillouin zone $\Gamma(\boldsymbol{k}=0)$ as following: $19A_g + 17B_g + 14A_u + 19B_u$ [32,33]. According to the selection rules, there are 36 Raman-active modes ($19A_g + 17B_g$) and 33 IR-active ones ($14A_u + 19B_u$). Among the Raman-active modes, 18 ones ($11A_g + 7B_g$) are the internal ones, corresponding to the vibrations of the $[MoO_4]^{2-}$ tetrahedra: symmetric stretching (ν_1, $2A_g$), anti-symmetric stretching (ν_3, $3A_g + 3B_g$), symmetric bending (ν_2, $3A_g + 1B_g$), and anti-symmetric stretching (ν_4, $3A_g + 3B_g$).

We have measured the polarized Raman spectra for three orientations of Yb:$MgMoO_4$ when cutting it along the ***a***-, ***b***- and ***c***-axes, as presented in Fig. 6. For labeling the geometry, we employed Porto's notations, *m*(*nl*)*k*, where *m* and *k* stand for the direction of propagation of the excitation and scattered light, respectively, and *n* and *l* are the corresponding polarization states. One can see that the Raman spectra of Yb:$MgMoO_4$ feature intense peaks located within two ranges of distinct wavenumbers, at 115 – 450 cm^{-1} and 750 – 1050 cm^{-1}, which is typical for simple and complex tungstate and molybdate crystals [34-36]. Within the low-wavenumber range, the bands arise from the lattice vibrations and some bending modes (ν_2 and ν_4) mixed with the former

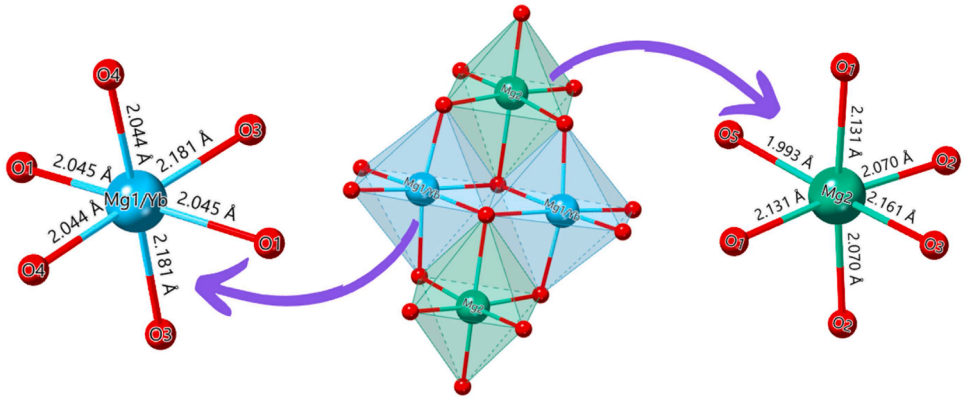

Fig. 4. The criss-cross structural unit in Yb:$MgMoO_4$ and the anionic coordination environment of Mg(1)|Yb and Mg(2) ions.

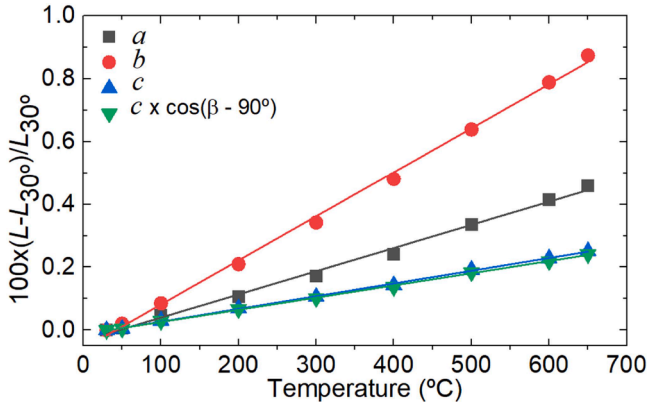

Fig. 5. Thermal evolution of the normalized unit-cell parameters of Yb:$MgMoO_4$, with $L = a, b, c$ and $c \times \cos(\beta - 90^\circ)$.

ones. The Raman peaks at high wavenumbers are mainly due to the stretching (ν_1 and ν_3) vibrations of the $[MoO_4]^{2-}$ tetrahedra. The mode at 957 cm^{-1} dominates in the spectra while the highest phonon energy mode is found at 969 cm^{-1}. These peaks are assigned to symmetric stretching (ν_1, $2A_g$) vibrations. The Raman peak linewidth (FWHM) at 957 cm^{-1} reaches ~ 7 cm^{-1}. The peak positions and linewidths are consistent with those for Tm:$MgMoO_4$ [23]. The Raman spectrum of undoped $MgMoO_4$ contains the same peaks in the range of 115–450 cm^{-1}, except for the fact that the peak at ~325 cm^{-1} is split into three components [32].

3.5. Optical spectroscopy of Yb^{3+} ions

The unpolarized overview absorption spectrum of the 0.2 at. % Yb:$MgMoO_4$ crystal is shown in Fig. 7(a). One can note a broad and intense absorption band with a maximum at ~500 nm which is causing the amber-like coloration of the crystal. It has been shown earlier [23] that the corresponding color centers are most likely related to molybdenum vacancies. This conclusion was made from the fact that the coloration of $MgMoO_4$ crystals almost completely disappears after prolonged annealing in air atmosphere containing pronounced amounts of MoO_3

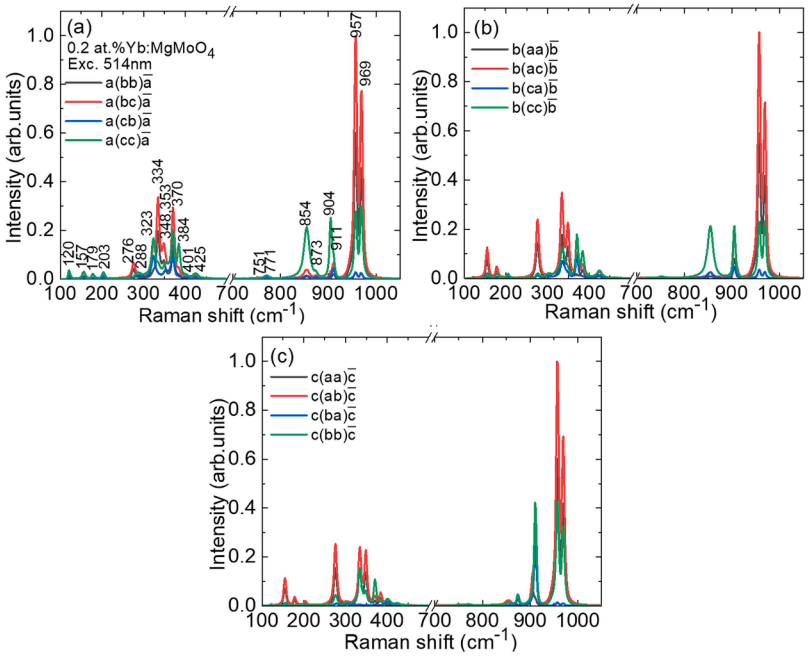

Fig. 6. Polarized Raman spectra of (a) ***a***-cut, (b) ***b***-cut and (c) ***c***-cut 0.2 at. % Yb:$MgMoO_4$ crystals, $\lambda_{exc} = 514$ nm, $T = 300$ K. *Numbers* in (a) - peak frequencies in cm^{-1}.

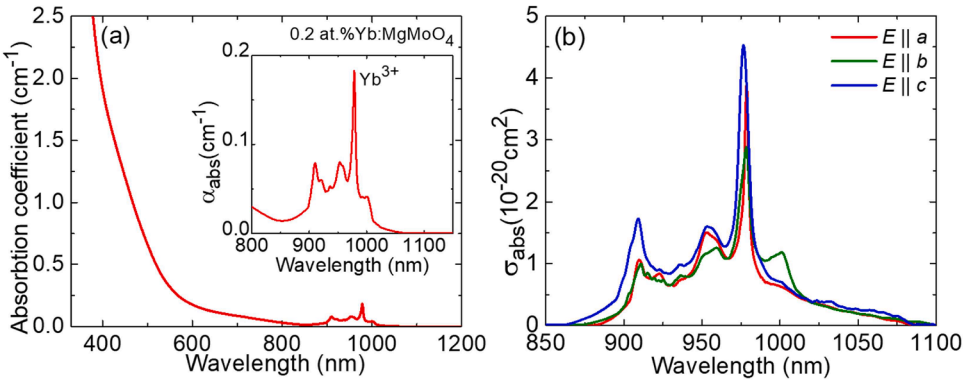

Fig. 7. Optical absorption of the 0.2 at. % Yb: $MgMoO_4$ crystal at room temperature: (a) an overview unpolarized absorption spectrum, *inset* – absorption of Yb^{3+} ions around 1 μm; (b) absorption cross-sections, σ_{abs}, of Yb^{3+} ions for light polarizations ***E*** || ***a, b, c***.

vapors, whereas annealing at similar temperatures and durations, but only in air atmosphere without MoO_3 does not change the crystal color.

The absorption near 1 μm is due to the Yb^{3+} ions (the $^2F_{7/2} \rightarrow {}^2F_{5/2}$ electronic transition). The RT polarized absorption spectra near 1 μm are shown in Fig. 7(b). They span from ~0.85 to 1.10 μm with an intense distinct peak at ~ 975 nm, corresponding, evidently, to the transition between the lowest Stark sub-levels of the ground state $^2F_{7/2}$ and the excited state $^2F_{5/2}$ of Yb^{3+} ions (the so-called zero-phonon line, ZPL).

For the $^2F_{7/2} \rightarrow {}^2F_{5/2}$ Yb^{3+} transition, at the ZPL, the peak absorption cross-sections σ_{abs} amount to 3.90×10^{-20} cm^2 at 978.6 nm for light polarization ***E*** || ***a*** (the absorption linewidth, full width at half maximum, FWHM is 4.5 nm), 2.89×10^{-20} cm^2 at 978.4 nm for ***E*** || ***b*** (FWHM = 11.3 nm) and 4.53×10^{-20} cm^2 at 976.5 nm for ***E*** || ***c*** (FWHM = 8.7 nm). Note that the absorption ZPL of Yb^{3+} ions in this crystal has a multi-peak structure even at RT and it is relatively broad. These peak σ_{abs} values are comparable with those for the Yb:$MgWO_4$ crystal ($\sigma_{abs} = 6.16 \times 10^{-20}$ cm^2 at 974.0 nm corresponding to an absorption bandwidth of 5.6 nm for light polarization ***E*** || N_g, $N_g \wedge \boldsymbol{a} = 36.4°$) [24]. For Yb,Li:$ZnWO_4$, lower values were found: $\sigma_{abs} = 2.40 \times 10^{-20}$ cm^2 at 972.7 nm corresponding to a broader absorption bandwidth of 8.3 nm also for light polarization ***E*** || N_g, $N_g \wedge \boldsymbol{c} = 12.4°$) [8]. In [37], the maximum absorption cross-section for Yb^{3+} ions in Yb^{3+},K^+:$ZnWO_4$ is given without specifying the polarization, $\sigma_{abs} = 2.6 \times 10^{-20}$ cm^2 at ~972 nm.

The-stimulated emission (SE) cross-section, σ_{SE}, spectra corresponding to the $^2F_{5/2} \rightarrow {}^2F_{7/2}$ transition of Yb^{3+} ions in $MgMoO_4$ were calculated by means of the Füchtbauer–Ladenburg (F-L) formula based on the measured polarized luminescence spectra:

$$\sigma_{SE}^{i}(\lambda) = \frac{\lambda^5}{8\pi\langle n\rangle^2 \tau_{rad} c} \frac{W_i(\lambda)}{1\Big/3\sum_{j=a,b,c}\int \lambda W_j(\lambda) d\lambda}. \quad (3)$$

Here, λ denotes the wavelength of light, $<n>$ represents the average refractive index of the host matrix, c is the speed of light, τ_{rad} stands for the radiative lifetime of the $^2F_{5/2}$ Yb^{3+} manifold, $W_i(\lambda)$ signifies the luminescence spectrum which was calibrated accounting for the spectral response of the optical spectrum analyser, and $i = a, b, c$ indicates the principal light polarization. The factor of 1/3 stands for averaging over three principal polarizations of light.

The luminescence of Yb^{3+} ions in $MgMoO_4$ spans from 925 nm to 1125 nm. This crystal features a relatively strong polarization anisotropy of emission properties which underlines the possibility to obtain linearly polarized laser emission. In Fig. 8 is the computed σ_{SE} spectrum for the Yb:$MgMoO_4$ crystal. Yb^{3+} ions feature reabsorption at the laser wavelengths (a quasi-three-level laser scheme) and laser emission usually occurs at the wavelengths well above the ZPL transition. In the spectral range where laser operation is expected, the highest σ_{SE} is 0.76 $\times 10^{-20}$ cm^2 at 1031 nm and 0.46 $\times 10^{-20}$ cm^2 at 1067 nm for light polarization ***E*** || ***c***.

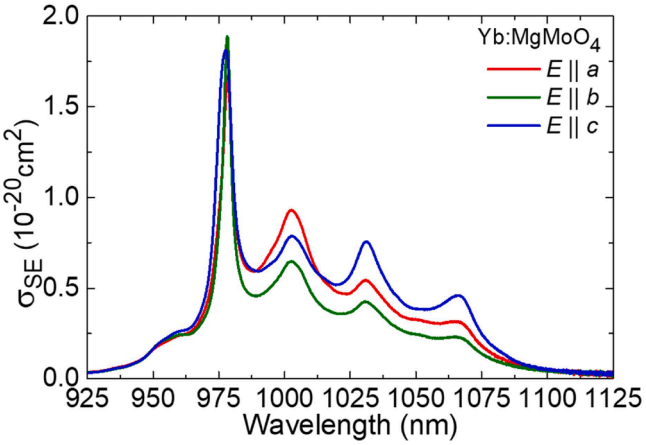

Fig. 8. Stimulated-emission cross-section, σ_{SE}, spectra of Yb^{3+} ions in $MgMoO_4$ for light polarizations ***E*** || ***a, b, c***.

Low-temperature (LT) absorption spectra were measured for light polarizations ***E*** || ***b*** and ***E*** || ***c***, see Fig. 9. The spectra indicate that, at 12 K, the above-mentioned absorption zero-phonon line splits into at least eight distinct components in the range of 972–980 nm. This may be evidence of the presence of Yb^{3+} ions in several structurally non-equivalent sites in the $MgMoO_4$ crystal. These sites can be regular magnesium positions Mg1 and Mg2 of the structure (see *Section 3.2*), as

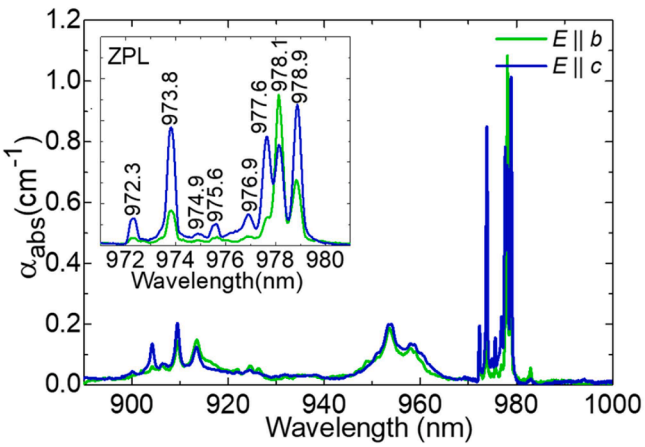

Fig. 9. LT (12 K) absorption spectra of Yb^{3+} ions in the 0.2 at. % Yb:$MgMoO_4$ crystal for light polarizations ***E*** || ***b*** and ***E*** || ***c***. *Inset* presents the structure of the ZPL in absorption, *numbers* – peak wavelengths in nm.

well as disturbed sites, correspond to associates of ytterbium with different kinds of charge compensators (cationic vacancies or accidental impurities, such as alkali ions, iron, silicon, *etc*.).

The low-temperature absorption spectra of Yb,Li:$ZnWO_4$ [8] do not indicate any splitting of the zero-phonon line. Simultaneously, this crystal features much higher segregation coefficient for Yb^{3+} ions, namely 0.25–0.5 depending on Li^+ concentration [18]. Thus, the substitution $Mg^{2+} \rightarrow Yb^{3+}$ is a less favorable process than the substitution $Zn^{2+} \rightarrow Yb^{3+}$, and one can expect the formation of various point defect associates, in contrast to the case of the $Zn^{2+} \rightarrow Yb^{3+}$ substitution, despite the fact that the ionic radii of Mg^{2+} and Zn^{2+} (and the average Mg-O and Zn-O interatomic distances) in the octahedral oxygen coordination are relatively close for the $MgMoO_4$ and $ZnWO_4$ crystals, see Table 2.

The LT (12 K) luminescence spectra of Yb:$MgMoO_4$ were also measured for light polarizations $\boldsymbol{E} \parallel \boldsymbol{b}$ and $\boldsymbol{E} \parallel \boldsymbol{c}$ (under non-selective excitation), see Fig. 10. Similar to the absorption spectra, one can also see eight sharp components of the split zero-phonon line of $^2F_{5/2} \rightarrow {}^2F_{7/2}$ transition of Yb^{3+} ions in the range of 972–980 nm. The shapes and the peak positions of the zero-phonon absorption and emission bands are consistent with each other except of the fact that the luminescence of the sharp lines at 978.1 nm and 978.9 nm is strongly suppressed by the reabsorption effect, or the used non-selective excitation wavelength poorly overlaps with the narrow absorption lines of the corresponding Yb^{3+} centers. Besides that, weaker and strongly split emission bands spanning from 1 μm to 1.08 μm corresponding to transitions to other (higher lying) Stark components of the $^2F_{7/2}$ ground state for various Yb^{3+} optical centers are visible.

We have also performed site-selective luminescence studies at 12 K, upon narrow-band excitation at different wavelengths (904.4, 909.6, 917.8, 933, and 976.6 nm). According to the results of these studies shown in Fig. 11, the groups of bands corresponding to Yb^{3+} centers located in at least five kinds of different, structurally non-equivalent crystallographic sites can be distinguished. The first one is efficiently excited at λ_{exc} = 904.4 nm (the transition from the lowest Stark component of the ground state to the highest component of the excited state) revealing a zero-phonon line at the wavelength of 972.5 nm. The second kind of Yb^{3+} centers is almost exclusively excited at λ_{exc} = 909.6 nm, whereas its emission ZPL appears at 973.7 nm. Three different kinds of Yb^{3+} centers were excited under the excitation at 917.8, 933.0 and 976.6 nm (the emission ZPLs at 977.6 nm, 978.1 nm and 978.9 nm). For revealing the structure of the observed Yb^{3+} centers, additional studies are required with use of electron paramagnetic resonance (EPR) and/or other kinds of measurements.

The luminescence decay from the $^2F_{5/2}$ state of Yb^{3+} ions in $MgMoO_4$ was further studied at RT, as shown in Fig. 12. It can be well described by the single-exponential law yielding a luminescence lifetime τ_{lum} of 0.63 ms. The luminescence lifetimes of Yb^{3+} in Yb:$MgWO_4$ and Yb,Li:$ZnWO_4$ are rather close, ~0.36–0.37 ms and ~ 0.366 ms [4,8]. This relatively long lifetime of Yb^{3+} upper laser level is expected to favor reaching low laser thresholds. The observation of a nearly single-exponential luminescence decay despite the evidence of multiple Yb^{3+} species in $MgMoO_4$ revealed by LT spectroscopic studies is most probably due to the close transition probabilities for these optical centers.

Table 2
Metal-to-oxygen interatomic distances for the $M^{2+}O_6$ octahedra in the $MgMoO_4$ and $ZnWO_4$ crystals.

$MgMoO_4$ (This work)				$ZnWO_4$ [38]	
[$Mg1O_6$]	Distance, Å	[$Mg2O_6$]	Distance, Å	[ZnO_6]	Distance, Å
Mg1-O1	2 × 2.0450	Mg2-O1	2 × 2.1310	Zn-O2	2 × 1.981
Mg1-O3	2 × 2.1808	Mg2-O2	2 × 2.0700	Zn-O1	2 × 2.032
Mg1-O4	2 × 2.0442	Mg2-O3	2.1612	Zn-O1	2 × 2.319
		Mg2-O5	1.9933		
Average	2.0900	Average	2.09275	Average	2.111

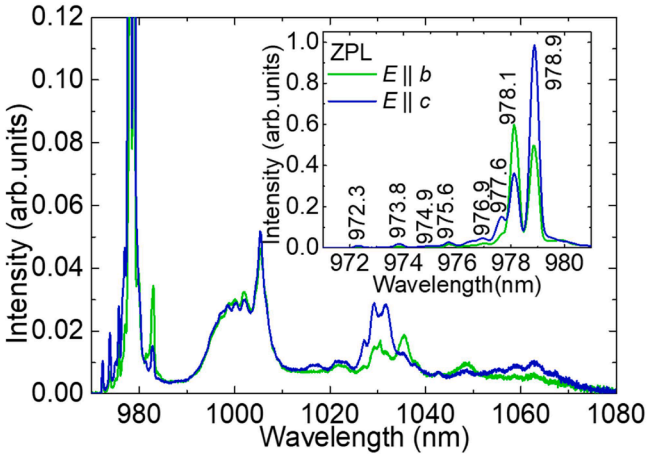

Fig. 10. LT (12 K) luminescence spectra of Yb^{3+} ions in the 0.2 at. % Yb:$MgMoO_4$ crystal for light polarizations $\boldsymbol{E} \parallel \boldsymbol{b}$ and $\boldsymbol{E} \parallel \boldsymbol{c}$. *Inset* – a close look at the ZPL structure, *numbers* – peak wavelengths in nm. Non-selective excitation.

4. Conclusions

In the present work, being motivated by the recent success of Yb^{3+}-doped monoclinic magnesium monotungstate crystal, $MgWO_4$, in ultrashort-pulse lasers at 1 μm, we focused our attention on its monomolybdate counterpart, Yb^{3+}:$MgMoO_4$, owing to its congruent melting allowing for the growth of large volume crystals by the Czochralski method. 0.2 at. % Yb:$MgMoO_4$ crystal with a high optical quality and only a weak amber-like coloration was grown and its structure was refined by the Rietveld method. This monomolybdate compound belongs to the monoclinic class (sp. gr. *C2/m*) and features a structure disorder due to two non-equivalent substitutional Mg^{2+} sites. The segregation coefficient of Yb^{3+} in $MgMoO_4$ is however relatively low, ~0.03, which is assigned to the difference in the ionic radii, charge and chemical nature of Mg^{2+} and Yb^{3+}. We believe that it could be further improved by codoping the crystal with proper charge compensators (*e.g.*, Li^+), which would be essential for the laser development.

The absorption and emission properties of Yb^{3+} ions in $MgMoO_4$ were studied for polarized light. This crystal exhibits a notable spectral line broadening at room temperature leading to broadband and almost structureless spectral gain profiles above 1 μm. In this regard, it even outperforms the Yb^{3+}:$MgWO_4$ crystal. This underlines the potential of the studied monomolybdate for 1-μm femtosecond lasers. To reveal the nature of this spectral line broadening, we employed site-selective spectroscopy at cryogenic temperatures (12 K). The multi-site behavior of rare-earth ions in $MgMoO_4$ was revealed for the first time. A variety of Yb^{3+} species comprising at least five non-equivalent optical centers was revealed. These centers can be regular magnesium positions Mg1 and Mg2 of the structure, as well as disturbed sites, corresponding to associates of ytterbium with different kinds of charge compensators (oxygen vacancies or accidental impurities, such as alkali ions). The intentional codoping, *e.g.*, with Li^+ ions, could reduce the number of optical centers or change their relative concentrations. This work extends the understanding of rare-earth doping mechanisms in monoclinic $M^{2+}XO_4$ crystals (where M = Mg, Zn and X = *W*, Mo) and the obtained information would allow engineering the gain bandwidth of Yb^{3+} ions to support the generation of sub-100 fs pulses. The latter could involve the growth of "mixed" Yb:Mg(W,Mo)O_4 crystals.

CRediT authorship contribution statement

Ghassen Zin Elabedine: Writing – original draft, Investigation.

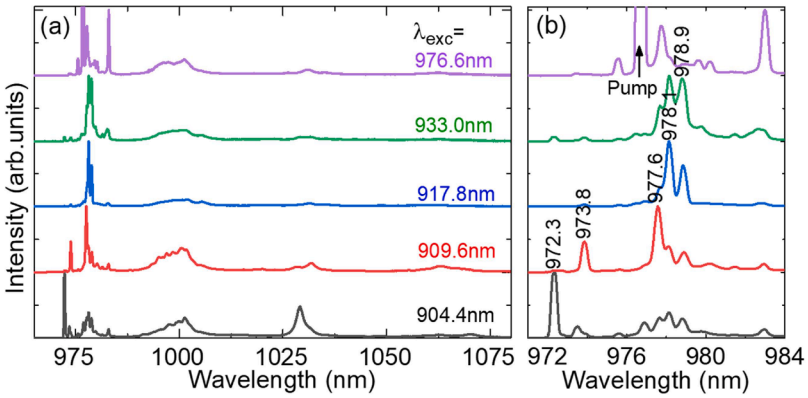

Fig. 11. LT (12 K) luminescence spectra of Yb^{3+} ions in the 0.2 at. % Yb:$MgMoO_4$ crystal measured under different excitation wavelengths λ_{exc}: (a) full spectra; (b) a close look at the ZPL transition.

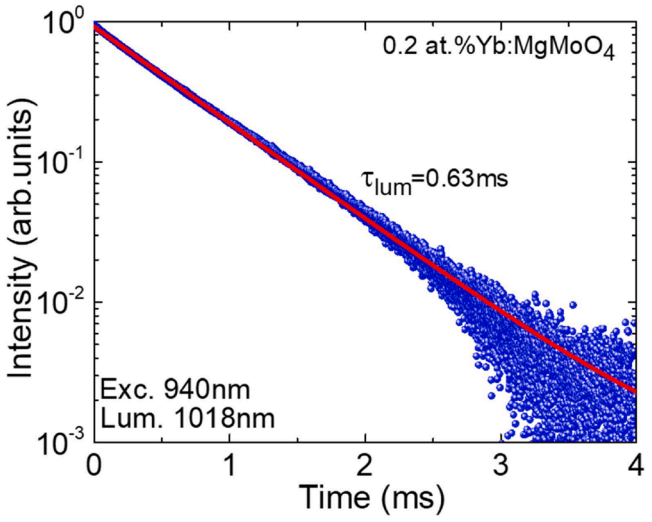

Fig. 12. Luminescence decay curve from the $^2F_{5/2}$ Yb^{3+} manifold in the 0.2 at. % Yb:$MgMoO_4$ crystal (finely powdered sample).

Yana S. Didenko: Writing – original draft, Investigation. **Pavel Loiko:** Writing – original draft, Methodology, Conceptualization. **Kirill A. Subbotin:** Writing – original draft, Investigation. **Anatolii I. Titov:** Investigation. **Liudmila D. Iskhakova:** Investigation. **Denis A. Lis:** Investigation. **Sergei K. Pavlov:** Investigation. **Yulia I. Zimina:** Investigation. **Kristina V. Kuleshova:** Investigation. **Rosa Maria Solé:** Methodology. **Magdalena Aguiló:** Supervision, Funding acquisition. **Francesc Díaz:** Supervision, Funding acquisition. **Patrice Camy:** Supervision. **Xavier Mateos:** Writing – review & editing, Supervision, Funding acquisition.

Declaration of competing interest

The authors declare that they have no known competing financial interests or personal relationships that could have appeared to influence the work reported in this paper.

Acknowledgements

The research was supported by the Russian Scientific Fund (grant No 23-22-00416); Grant PID2022-141499OB-100 of the Spanish Government funded by MICIU/AEI/10.13039/ 501100011033/ and by FEDER/ UE.

Data availability

Data will be made available on request.

References

[1] A.A. Lagatsky, C.T.A. Brown, W. Sibbett, Highly efficient and low threshold diode-pumped Kerr-lens mode-locked Yb:KYW laser, Opt. Express 12 (2004) 3928–3933, https://doi.org/10.1364/OPEX.12.003928.
[2] U. Griebner, S. Rivier, V. Petrov, M. Zorn, G. Erbert, M. Weyers, X. Mateos, M. Aguiló, J. Massons, F. Díaz, Passively mode-locked Yb:$KLu(WO_4)_2$ oscillators, Opt. Express 13 (2005) 3465–3470, https://doi.org/10.1364/OPEX.13.003465.
[3] Ò. Silvestre, J. Grau, M.C. Pujol, J. Massons, M. Aguiló, F. Díaz, M.T. Borowiec, A. Szewczyk, M.U. Gutowska, M. Massot, A. Salazar, V. Petrov, Thermal properties of monoclinic $KLu(WO_4)_2$ as a promising solid state laser host, Opt. Express 16 (2008) 5022–5034, https://doi.org/10.1364/OE.16.005022.
[4] P. Loiko, M. Chen, J.M. Serres, M. Aguiló, F. Díaz, H. Lin, G. Zhang, L. Zhang, Z. Lin, P. Camy, S.-B. Dai, Z. Chen, Y. Zhao, L. Wang, W. Chen, U. Griebner, V. Petrov, X. Mateos, Spectroscopy and high-power laser operation of a monoclinic Yb^{3+}:$MgWO_4$ crystal, Opt. Lett. 45 (2020) 1770–1773, https://doi.org/10.1364/OL.389627.
[5] L. Zhang, L. Basyrova, P. Loiko, P. Camy, Z. Lin, G. Zhang, S. Slimi, R.M. Solé, X. Mateos, M. Aguiló, F. Díaz, E. Dunina, A. Kornienko, U. Griebner, V. Petrov, L. Wang, W. Chen, Growth, structure, and polarized spectroscopy of monoclinic Er^{3+}:$MgWO_4$ crystal, Opt. Mater. Express 12 (2022) 2028–2040, https://doi.org/10.1364/OME.449649.
[6] L. Zhang, P. Loiko, J.M. Serres, E. Kifle, H. Lin, G. Zhang, E. Vilejshikova, E. Dunina, A. Kornienko, L. Fomicheva, U. Griebner, V. Petrov, Z. Lin, W. Chen, K. Subbotin, M. Aguiló, F. Díaz, X. Mateos, Growth, spectroscopy and first laser operation of monoclinic Ho^{3+}:$MgWO_4$ crystal, J. Lumin. 213 (2019) 316–325, https://doi.org/10.1016/j.jlumin.2019.04.035.
[7] L. Zhang, H. Lin, G. Zhang, X. Mateos, J.M. Serres, M. Aguiló, F. Díaz, U. Griebner, V. Petrov, Y. Wang, P. Loiko, E. Vilejshikova, K. Yumashev, Z. Lin, W. Chen, Crystal growth, optical spectroscopy and laser action of Tm^{3+}-doped monoclinic magnesium tungstate, Opt. Express 25 (2017) 3682–3693, https://doi.org/10.1364/OE.25.003682.
[8] A. Volokitina, S.P. David, P. Loiko, K. Subbotin, A. Titov, D. Lis, R.M. Solé, V. Jambunathan, A. Lucianetti, T. Mocek, P. Camy, W. Chen, U. Griebner, V. Petrov, M. Aguiló, F. Díaz, X. Mateos, Monoclinic zinc monotungstate Yb^{3+},Li^{+}:$ZnWO_4$: Part II. Polarized spectroscopy and laser operation, J. Lumin. 231 (2021) 117811, https://doi.org/10.1016/j.jlumin.2020.117811.
[9] Z. Xia, F. Yang, L. Qiao, F. Yan, End pumped yellow laser performance of Dy^{3+}:$ZnWO_4$, Opt. Commun. 387 (2017) 357–360, https://doi.org/10.1016/j.optcom.2016.12.008.
[10] F. Yang, C. Tu, The spectroscopy investigation of $ZnWO_4$:Tm^{3+} single crystal, J. Alloys Compd. 535 (2012) 83–86, https://doi.org/10.1016/j.jallcom.2012.04.084.
[11] H. Lin, G. Zhang, L. Zhang, Z. Lin, F. Pirzio, A. Agnesi, V. Petrov, W. Chen, Continuous-wave and SESAM mode-locked femtosecond operation of a Yb:$mgWO_4$ laser, Opt. Express 25 (2017) 11827–11832, https://doi.org/10.1364/OE.25.011827.
[12] Y. Wang, W. Chen, M. Mero, L. Zhang, H. Lin, Z. Lin, G. Zhang, F. Rotermund, Y. J. Cho, P. Loiko, X. Mateos, U. Griebner, V. Petrov, Sub-100 fs Tm:$MgWO_4$ laser at 2017 nm mode locked by a graphene saturable absorber, Opt. Lett. 42 (2017) 3076–3079, https://doi.org/10.1364/OL.42.003076.
[13] L. Zhang, Y. Huang, S. Sun, F. Yuan, Z. Lin, G. Wang, Thermal and spectral characterization of Cr^{3+}:$MgWO_4$ - a promising tunable laser material, J. Lumin. 169 (2016) 161–164, https://doi.org/10.1016/j.jlumin.2015.08.078.
[14] P. Loiko, Y. Wang, J.M. Serres, X. Mateos, M. Aguiló, F. Díaz, L. Zhang, Z. Lin, H. Lin, G. Zhang, E. Vilejshikova, E. Dunina, A. Kornienko, L. Fomicheva, V. Petrov, U. Griebner, W. Chen, Monoclinic Tm:$MgWO_4$ crystal: crystal-field

analysis, tunable and vibronic laser demonstration, J. Alloys Compd. 763 (2018) 581–591, https://doi.org/10.1016/j.jallcom.2018.05.237.
[15] X. Wang, Z. Fan, H. Yu, H. Zhang, J. Wang, Characterization of $ZnWO_4$ Raman crystal, Opt. Mater. Express 7 (2017) 1732–1744, https://doi.org/10.1364/OME.7.001732.
[16] T.T. Basiev, A.Y. Karasik, A.A. Sobol, D.S. Chunaev, V.E. Shukshin, Spontaneous and stimulated Raman scattering in $ZnWO_4$ crystals, Quantum Electron. 41 (2011) 370–372, https://doi.org/10.1070/QE2011v041n04ABEH014527.
[17] G.Z. Elabedine, K. Subbotin, P. Loiko, Y. Zimina, S. Pavlov, A. Titov, P. Camy, A. Braud, R.M. Solé, M. Aguiló, F. Díaz, W. Chen, X. Mateos, V. Petrov, Monoclinic Yb^{3+},Li^{+}:$ZnWO_4$ - efficient broadly emitting laser material, Proc. SPIE 12864 (2024) 128640K, https://doi.org/10.1117/12.3002431.
[18] K.A. Subbotin, A.I. Titov, S.K. Pavlov, P.A. Volkov, V.V. Sanina, D.A. Lis, O.N. Lis, Y.I. Zimina, Y.S. Didenko, E.V. Zharikov, Effect of Li^{+} codoping on the mechanical strength of YB:$ZnWO_4$ single crystals, J. Cryst. Growth. 582 (2022) 126498, https://doi.org/10.1016/j.jcrysgro.2021.126498.
[19] K.I. Gerasimov, M.M. Minnegaliev, S.A. Moiseev, K.A. Subbotin, S.K. Pavlov, Laser site selective spectroscopy of Er^{3+} in $ZnWO_4$ single crystal, Magn. Reson. Solids vol. 26 (2024) 24204, https://doi.org/10.26907/mrsej-24202.
[20] G. Zin Elabedine, R.M. Solé, S. Slimi, M. Aguiló, F. Díaz, W. Chen, V. Petrov, X. Mateos, Growth, anisotropy, and spectroscopy of Tm^{3+} and Yb^{3+} doped $MgWO_4$ crystals, CrystEngComm (2025), https://doi.org/10.1039/D4CE01168F.
[21] L. Li, Y. Huang, L. Zhang, Z. Lin, G. Wang, Growth, mechanical, thermal and spectral properties of Cr^{3+}:$MgMoO_4$ crystal, PLoS ONE 7 (2012) e30327, https://doi.org/10.1371/journal.pone.0030327.
[22] E. Cavalli, A. Belletti, M.G. Brik, Optical spectra and energy levels of the Cr^{3+} ions in MWO_4 (M=Mg, Zn, Cd) and $MgMoO_4$ crystals, J. Phys. Chem. Solids. 69 (2008) 29–34, https://doi.org/10.1016/j.jpcs.2007.07.101.
[23] K. Subbotin, A. Titov, D. Lis, Y. Zimina, Y. Didenko, G.Z. Elabedine, K. Eremeev, R. M. Solé, M. Aguiló, P. Volkov, P. Popov, E. Chernova, F. Díaz, P. Camy, P. Loiko, X. Mateos, Growth, structure refinement, thermal expansion and optical spectroscopy of Tm^{3+}-doped $MgMoO_4$, Opt. Mater. 138 (2023) 113648, https://doi.org/10.1016/j.optmat.2023.113648.
[24] D.A. Spasskii, V.N. Kolobanov, V.V. Mikhaĭlin, L.Y. Berezovskaya, L.I. Ivleva, I. S. Voronina, Luminescence peculiarities and optical properties of $MgMoO_4$ and $MgMoO_4$:Yb crystals, Opt. Spectrosc. 106 (2009) 556–563, https://doi.org/10.1134/S0030400X09040171 [Transl. from Optika i Spektroskopiya 106 (2009) 625–632].
[25] K.A. Subbotin, Y.S. Didenko, A.I. Titov, D.A. Lis, S.K. Pavlov, P.A. Volkov, K. I. Runina, V.V. Voronov, E.V. Chernova, O.N. Lis, K.V. Kuleshova, Y.I. Zimina, Influence of ultrahigh dilution treatment of the charge on the growth and spectroscopic properties of Nd:$MgMoO_4$ potential laser crystal, Cryst 14 (2024) 100, https://doi.org/10.3390/cryst14010100.
[26] V.V. Bakakin, R.F. Klevtsova, L.A. Gaponenko, Crystal structure of magnesium molybdate $MgMoO_4$-an example of modified closest packing with two types of tetrahedra, Kristallografiya 27 (1982) 38–42.
[27] W. Ran, L. Wang, M. Yang, X. Kong, D. Qu, J. Shi, Enhanced energy transfer from Bi^{3+} to Eu^{3+} ions relying on the criss-cross cluster structure in $MgMoO_4$ phosphor, J. Lumin. 192 (2017) 141–147, https://doi.org/10.1016/j.jlumin.2017.06.039.
[28] V.B. Mikhailik, H. Kraus, V. Kapustyanyk, M. Panasyuk, Y. Prots, V. Tsybulskyi, L. Vasylechko, Structure, luminescence and scintillation properties of the$MgWO_4$–$MgMoO_4$ system, J. Phys. Condens. Matter. 20 (2008) 365219, https://doi.org/10.1088/0953-8984/20/36/365219.
[29] L.Y. Zhou, J.S. Wei, L.H. Yi, F.Z. Gong, J.L. Huang, W. Wang, A promising red phosphor $MgMoO_4$:Eu^{3+} for white light emitting diodes, Mater. Res. Bull. 44 (2009) 1411–1414, https://doi.org/10.1016/j.materresbull.2008.11.019.
[30] V.F. Tarasov, A.A. Sukhanov, E.V. Zharikov, K.A. Subbotin, D.A. Lis, EPR spectroscopy of impurity ytterbium ions in synthetic forsterite single crystals, Appl. Magn. Reson. 53 (2022) 1211–1226, https://doi.org/10.1007/S00723-021-01453-9.
[31] L.P. Litovkina, Electron paramagnetic resonance of ions of the 3d and 4f-groups in single crystals of $MgMoO_4$, J. Struct. Chem. 7 (1967) 575–577, https://doi.org/10.1007/BF00743558.
[32] M.N. Coelho, P.T.C. Freire, M. Maczka, C. Luz-Lima, G.D. Saraiva, W. Paraguassu, A.G. Souza Filho, P.S. Pizani, High-pressure Raman scattering of $MgMoO_4$, Vib. Spectrosc. 68 (2013) 34–39, https://doi.org/10.1016/j.vibspec.2013.05.007.
[33] P.J. Miller, The Raman spectra of $MgMoO_4$, Spectrochim. Acta Part A 27 (1971) 957–960, https://doi.org/10.1016/0584-8539(71)80178-2.
[34] V.V. Atuchin, O.D. Chimitova, T.A. Gavrilova, M.S. Molokeev, S.J. Kim, N. V. Surovtsev, B.G. Bazarov, Synthesis, structural and vibrational properties of microcrystalline $RbNd(MoO_4)_2$, J. Cryst. Growth. 318 (2011) 683–686, https://doi.org/10.1016/j.jcrysgro.2010.09.076.
[35] V.V. Atuchin, A.S. Aleksandrovsky, O.D. Chimitova, A.S. Krylov, M.S. Molokeev, B. G. Bazarov, J.G. Bazarova, Z. Xia, Synthesis and spectroscopic properties of multiferroic β'-$Tb_2(MoO_4)_3$, Opt. Mater. 36 (2014) 1631–1635, https://doi.org/10.1016/j.optmat.2013.12.008.
[36] C.S. Lim, A. Aleksandrovsky, M. Molokeev, A. Oreshonkov, V. Atuchin, Microwave sol–gel synthesis and upconversion photoluminescence properties of $CaGd_2(WO_4)_4$: Er^{3+}/Yb^{3+} phosphors with incommensurately modulated structure, J. Solid State Chem. 228 (2015) 160–166, https://doi.org/10.1016/j.jssc.2015.04.032.
[37] F. Yang, The spectroscopic investigation of $ZnWO_4$:Yb^{3+} single crystal, J. Mater. Res. 27 (2012) 2096–2100, https://doi.org/10.1557/jmr.2012.126.
[38] K. Subbotin, P. Loiko, S. Slimi, A. Volokitina, A. Titov, D. Lis, E. Chernova, S. Kuznetsov, R.M. Solé, U. Griebner, V. Petrov, M. Aguiló, F. Díaz, P. Camy, E. Zharikov, X. Mateos, Monoclinic zinc monotungstate Yb^{3+},Li^{+}:$ZnWO_4$: Part I. Czochralski growth, structure refinement and Raman spectra, J. Lumin. 228 (2020) 117601, https://doi.org/10.1016/j.jlumin.2020.117601.